3D Surface Modeling and Measuring System for Pneumatic Caisson

Baoshun Li[1]; Qixin Cao[2]; Lei Zhang[3]; Jay Lee[4]; Chuntao Leng[5]; and Yaoliang Li[6]

Abstract: In order to build a 3D model environment of a pneumatic caisson for excavator operators and managers, a modeling and measuring 3D surface system of unmanned pneumatic caisson was presented in this paper. The whole system is based on two 3D laser scanners for the pneumatic caisson by acquiring the surface data of pneumatic caisson and successive data processing for surface reconstruction and measurement. Registration and reconstruction are also discussed in this paper. In order to convert two point sets into one common coordinate, Hough transforms were used to extract planes and then by using their parameters to register the two point sets. As for surface reconstruction using triangular meshing, a new method based on curves was presented. When combined with the real-time pose and location of the excavators, the 3D environment can be used as a "virtual reality" operating environment for excavation operators. The whole system has been applied in a pneumatic caisson of an underground project in a Shanghai subway, which proved to be working well, with less than 16-s work cycle (period of a single 180° 3D laser scan), at an estimated resolution of less than 20 mm.

DOI: 10.1061/(ASCE)CP.1943-5487.0000023

CE Database subject headings: Caissons; Data processing; Measurement; Three-dimensional models.

Author keywords: Pneumatic caisson; 3D laser scanner; Real time; Data registration; Surface reconstruction; 3D measurement.

Introduction

Backgrounds

In the unmanned pneumatic caisson method (Kodaki et al. 1997; Peng et al. 2003), there is an increasingly demand for 3D surface reconstruction and measurement of the pneumatic caisson in real time. As for excavation operators, they prefer to operate the excavators in a 3D environment instead of the current 2D camera environment. Currently, in order to remotely operate excavators safely and avoid excavators collision with other objects, many cameras are installed in different locations of the working chamber of the pneumatic caisson at different viewpoints. Excavation workers also have to fully concentrate on the operation via multiple TV monitors which could result in fatigue and low work efficiency. On the other hand, mishandling frequently occurs, which may result in collisions between two excavators. As for managers, even researchers on pneumatic caisson, surface configuration in working chamber has an important influence not only on caisson subsiding but also on the daily process management. With a detailed real-time 3D height map like the digital evaluation model in cartology, "refined excavation" or "refined management" for pneumatic caisson can be achieved. This can help to improve the schedule of soil removal and improve decision making as to how much and which part of the surface of the pneumatic should be removed first. Researchers on pneumatic caisson can also measure the surface profile of the work chamber of the pneumatic caisson, so that they study the relationship between the excavation process and the subsidence of the pneumatic caisson. All of these need a real-time 3D surface reconstruction and measurement system. Although many current commercial devices can perform data acquisition, reconstruction, or measurement, very few systems suffice to the specific demands of a building 3D environment for the pneumatic caisson. Therefore, there is a demand for a special device for the 3D data acquisition, reconstruction, and measurement of pneumatic caissons.

Goal and Requirement

Our basic goal is to develop a 3D laser scanner system meeting the demand of the environment of pneumatic caissons which can measure the working chamber surface in real time, providing a real 3D environment and friendly interface for operators and managers. Because of the low speed and the occlusion problems of a 3D laser scanner, it is impractical to build a real-time 3D model for moving excavators. But when the real-time pose and location of the excavators are acquired by using positioning sensors and angular transducers, the system can rebuild excavator models in a

[1]Research Institute of Robotics, School of Mechanical Engineering, Shanghai JiaoTong Univ., 800 Dongchuan Rd., Shanghai 200240, People's Republic of China (corresponding author). E-mail: baoshunleo@sjtu.org

[2]Research Institute of Robotics, School of Mechanical Engineering, Shanghai JiaoTong Univ., 800 Dongchuan Rd., Shanghai 200240, People's Republic of China. E-mail: qxcao@sjtu.edu.cn

[3]Research Institute of Robotics, School of Mechanical Engineering, Shanghai JiaoTong Univ., 800 Dongchuan Rd., Shanghai 200240, People's Republic of China. E-mail: zhanglei@sjtu.edu.cn

[4]Research Center of Intelligent Maintenance Systems, Univ. of Cincinnati, P.O. Box 210072, Cincinnati, OH 45221. E-mail: jaylee@uc.edu

[5]Research Institute of Robotics, School of Mechanical Engineering, Shanghai JiaoTong Univ., 800 Dongchuan Rd., Shanghai 200240, People's Republic of China. E-mail: ctleng@sjtu.edu.cn

[6]Shanghai Foundation Engineering Company, 406 Jiangxi Rd., Shanghai 200002, People's Republic of China. E-mail: liyaoliang@263.net

Note. This manuscript was submitted on June 28, 2008; approved on April 2, 2009; published online on April 13, 2009. Discussion period open until October 1, 2010; separate discussions must be submitted for individual papers. This paper is part of the ***Journal of Computing in Civil Engineering***, Vol. 24, No. 3, May 1, 2010. ©ASCE, ISSN 0887-3801/2010/3-223–240/$25.00.

real 3D surface environment. Our long-term goal of the project is to provide a 3D modeling and measuring environment based on our 3D laser scanner system which is able to not only replace the 2D camera environment completely but also provide a foundation for intelligent excavation robots.

Organization of the Paper

This paper is organized as follows: the section "Related Works" will discuss related works. "3D Surface Modeling and Measuring System for Pneumatic Caisson" gives a detailed description of the system and units used in the proposed 3D laser scanner system; "Registration Method Based on a Modified Hough Transform" discusses the registration method of 3D point sets based on Hough transforms (HT); "3D Surface Reconstruction Method" presents the curves segmentation and surface reconstruction based on curves. "Discussion and Analysis of Result" gives the results and analysis. "Conclusions" gives the conclusions.

Related Works

In recent years, there is a rapid growth of 3D technology. 3D laser scanners which can acquire real information of the surfaces of complex objects has been used in many fields, such as reverse engineering, historical heritage studies, medical sciences, and manufacturing (Arayici 2007; González et al. 2007; Levoy et al. 2000; Shih et al. 2007; Sithole and Vosselman 2006; Yahya Alshawbkeh and Haala 2005; Yu et al. 2007). Levoy et al. (2000) in their Digital Michelangelo Project have reconstructed some scanned models of sculptures. González et al. (2007) demonstrated an application of using a 3D scanner to study the evolution of an underwater sediment bed in real time. Shih et al. (2007) used a 3D digital scan to virtually "preserve" a historical temple. Arayici (2007) gave a detailed case study on a building a 3D model using terrestrial laser scanners. But very few 3D laser scanners are currently being used in pneumatic caissons.

3D laser scanners are made based on two types of principles [triangulation and time-of-flight (TOF)] (www.sick.com, www.riegl.com). The principle of triangulation relies on the projection of a light pattern, i.e., a line is projected by the laser over an object and captured by the digital camera. The distance from objects to system can be calculated by trigonometry, as long as a priori distance between the camera and laser is obtained (Frohlich and M 2006; Gregor and Whitaker 2001). The principle of TOF means to measure the span time of flight of laser light pulse: a pulsed laser beam is emitted and reflected if it meets an object. The reflection is registered by the scanner's receiver. The time between transmission and reception of the impulse is directly proportion to the distance between the scanner and the object (time of flight) (www.sick.com). There are many 3D laser scanners both based on the principle of triangulation and TOF available in current market, such as LMS-Z210, Cyrax2500, Optech ILRIS-3D, and other 3D laser scanners, which based on TOF. Cyberware, 3D scanner, Minolta, are based on triangulation (Frohlich and M 2006).

Although these products have many advantages, such as high accuracy, resolution, velocity, feasible software, their limitation makes it inconvenient for people to use in the case of the pneumatic caisson. For example, in order to avoid being destroyed by the moving excavators, generally, 3D laser scanners have to be placed in holes of the ceiling of the working chamber, as shown in Fig. 5. This results in limitations imposed while using of 3D laser scanners, such as occlusions and nonadjustable laser scanner range. Another limitation of commercial laser scanners is their invariable resolution, very expensive and a long scanning cycle.

Because of the increasing demand for 3D laser scanner in new arenas, as stated earlier, present-day commercial 3D laser scanners tend to be slow, expensive, and difficult to use and cannot satisfy those demands. Many researchers have developed many kinds of new 3D laser scanners. Rusinkiewicz et al. (2002) demonstrated a real-time acquisition 3D system. Tognola et al. (2003) developed a 3D laser scanner system with which they reconstruct a 3D model for a human heart. In order to overcome the heavy and limited size of commercial 3D laser scanner (Borghese et al. 1998) designed a flexible and portable 3D scanner. Most of these 3D laser scanners are designed for the specific uses of researchers and are not suitable for use with pneumatic caissons.

In this paper, we developed a 3D laser scanner which can be used for the pneumatic caisson. Then we built a 3D environment with real data of a pneumatic caisson and also incorporate the excavators' model into the 3D environment.

3D Surface Modeling and Measuring System for Pneumatic Caisson

The 3D surface modeling and measuring system for pneumatic caisson are shown in Fig. 1, which consists mainly of (1) a 3D laser scanner; (2) assistant measurement units (distance laser sensor, position transducer and inclination sensor); and (3) computer—a real-time data processor.

3D laser scanners scan the surface of the working chamber and transfer the data to a computer. The number of 3D laser scanners is determined by how many working chambers are in the pneumatic caisson and the volumetric size of the working chambers. Distance laser sensors and position transducers of the assistant measurement are used to determine the location and pose of the excavators. The inclination sensor is related to monitor the attitude of the pneumatic caisson. Computers in the ground control room control how and when to scan, convert the data into a 3D model, receive the user's instruction, and give the result of measurement.

A block diagram of the system architecture for the proposed pneumatic caisson system is also shown in Fig. 2. The whole system can be divided into four modules: (1) sensor module; (2) motion control module; (3) 3D segmentation and surface reconstruction module; and (4) excavator collision detection.

"Sway" Operation Mode and "Rotation" Operation Mode of 3D Laser Scanner

To develop a feasible and flexible 3D scanner for the pneumatic caisson, this section compares the operation modes of a 3D laser scanner. Generally, the excavating equipment move back and forth along its rails installed on the ceiling of the work chamber and may extend their manipulators into the entire workspace of the work chamber, the 3D laser scanner may need to be protected by installing it into a hole in the ceiling. This would result in a narrow field-of-view since it has to be installed into a small space thus restricting its field of motion. Also because of the specific conditions in the working chamber where the pneumatic caisson operates, such as high pressure, high humidity, high dust levels, and high temperature, we have found that no specific laser products are able to meet those requirements and be used in an uncontrolled environment.

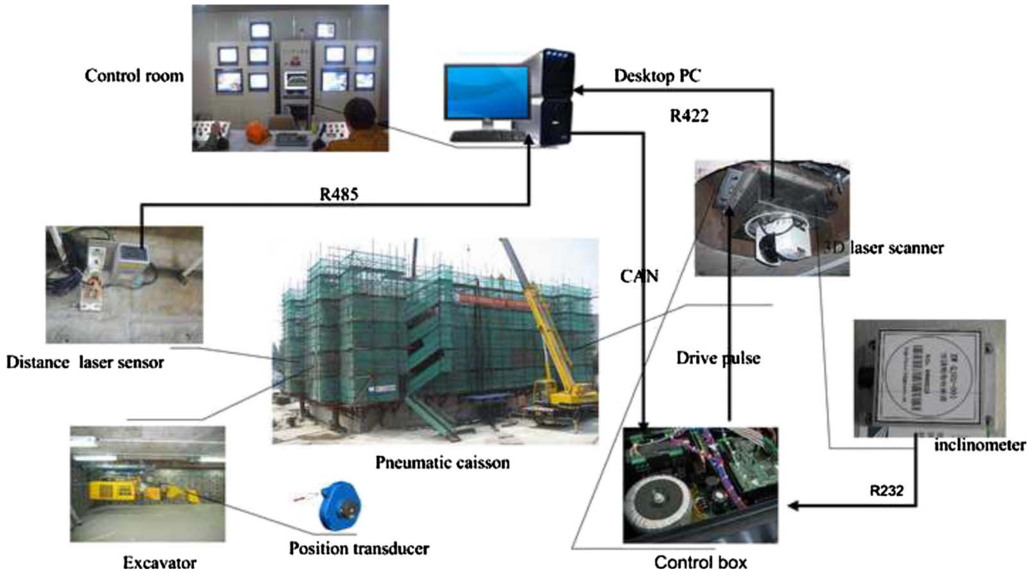

Fig. 1. Schematic diagram of the 3D surface modeling and measuring system for pneumatic caisson

Based on our survey with the current commercial 3D laser scanners, it is found that people generally build a 3D laser scanner using a 2D laser scanner sensor. There are two ways to build a 3D laser scanner with a 2D laser scanner sensor. The main difference between the two modes lies in their structures and operations. Here, we would like to introduce a naming convention where we call the operation mode of our system "rotation" and current commercial 3D laser's operation mode "sway." The principle of the Rotation operation mode is shown in Part A of Fig. 3; the pulsed laser beam is deflected with an angle of β by an internal mirror and a fan-shaped scan (line scan) is made in the scanning plane. The rotary scan (frame scan) is obtained by rotating the whole laser scanner sensor around the *z* axis with an angel of α ranging from 0 to 180°. We show the principle of the sway operation mode with a typical product-LMS-Z390, a product by RIEGL(in Part B of Fig. 3); the direction of the line scan is vertical, from top to bottom or vice versa, while the direction of the frame scan rotating the whole laser 360°. A 3D laser scanner with rotation operation mode generally has a wider view of field than that with the sway operation mode. For example, the view of field of RIEGL LMS-Z360i is $90° \times 360°$, however, our 3D laser scanner with rotation operation mode is $180° \times 360°$. The difference between these two kinds of range images obtained from the two modes of 3D laser scanners lies in their structures (as shown in Fig. 3): The scan lines of the rotation mode intersect at a common point with each other while the scan lines of the sway mode are disjointed and have no common axis. Fig. 3(c) shows a part of a range image obtained from a 3D laser scanner with rotation operation mode, which are composed of many concentric circles. The point density of the laser scanner with sway operation mode is more uniform than that with rotation operation mode. No-uniform point cloud brings about some disadvantages, such as redundant points around the axis of rotation [Fig. 3(c)], a large distance between points with a large value in two neighboring scan frames, which requires different methods of processing the data collected.

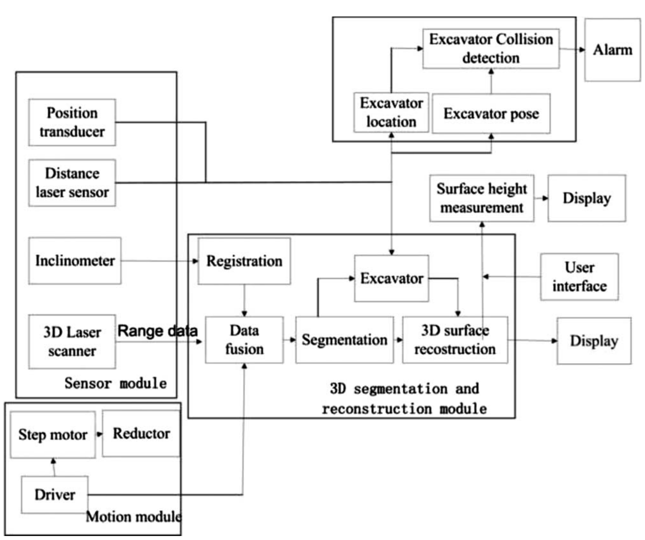

Fig. 2. Block diagram of the proposed architecture for 3D surface modeling and measuring system

To select the operation mode for a 3D laser scanner, we need to determine what its view of field and other requirements such as point density, speed, volumetric size, etc., are. In our case, excavators can extend their manipulators near the ceiling of the work chamber. We have to protect the 3D laser scanner and place it into a hole and we also need a wide view of the field so that the overall space inside the pneumatic caisson can be scanned; therefore, we build our 3D laser scanner with the rotation operation mode.

3D Laser Scanner for Pneumatic Caisson

The proposed 3D laser scanner unit based on the principle of the rotation mode is composed of a 2D laser scanner sensor, a step motor, a worm speed reducer, an inclinometer, a drive shaft, two limit switches, an optical fiber sensor, a control box and other miscellaneous parts such as a cover, two connector panels, mounting rack, sealing plate, etc. Fig. 4 shows scheme of the structure; Fig. 5 is the 3D laser scanner installed into the hole of the work chamber ceiling of a pneumatic caisson. In this paper, a high-quality 2D laser sensor product (SICK, LMS-290, 180° coverage, 10-mm resolution, measurements distance up to 80 m,

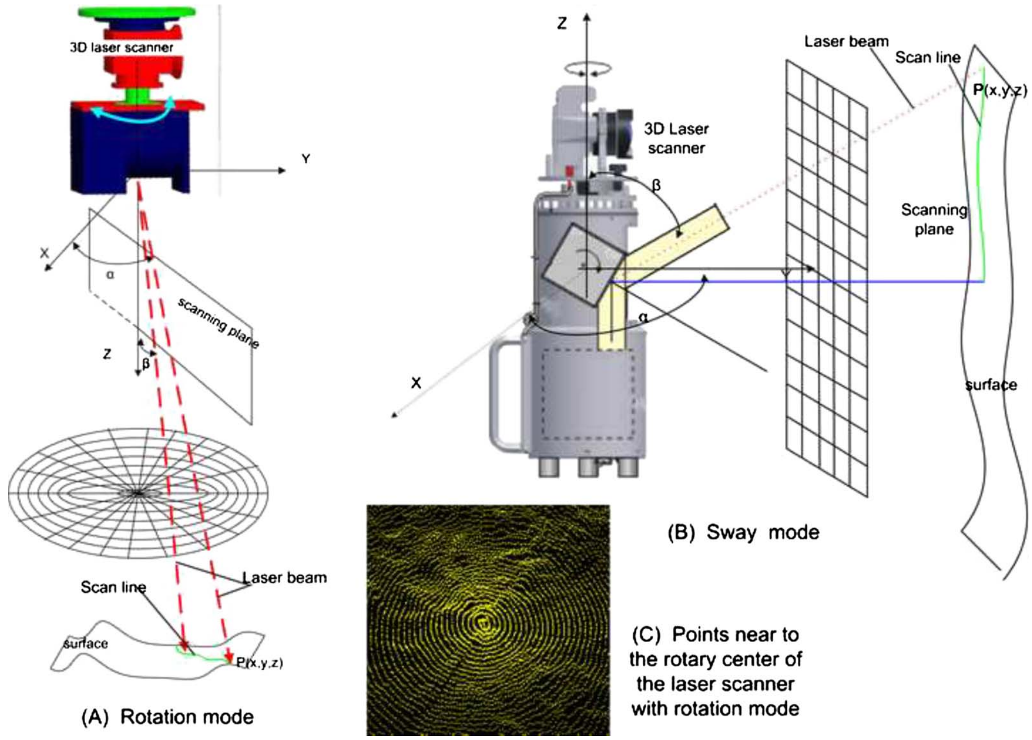

Fig. 3. Schematic diagram of 3D laser scanner with rotation mode and with sway mode

R422/R232 data interface) (www.sick.com) is selected as the primary sensor, which works well under 0.4-MPa air pressure (relative pressure) and can meet the requirements for operation with a pneumatic caisson. In order to drive the 2D scanned laser sensor with pinpoint accuracy and adjustable speed control, the step motor and the worm speed reducer are used. The optical fiber sensor acts as a zero point for calibration and two limit switches ensure the safety of the laser sensor during rotation. The 2D laser sensor is driven by a stepper motor which rotates the laser sensor from 0° (zero point) to 180° (endpoint) or from 180° to 0° about the drive shaft. We define the time taken by the stepper motor to complete the aforementioned 180° 3D scan as a work cycle (Fig. 4).

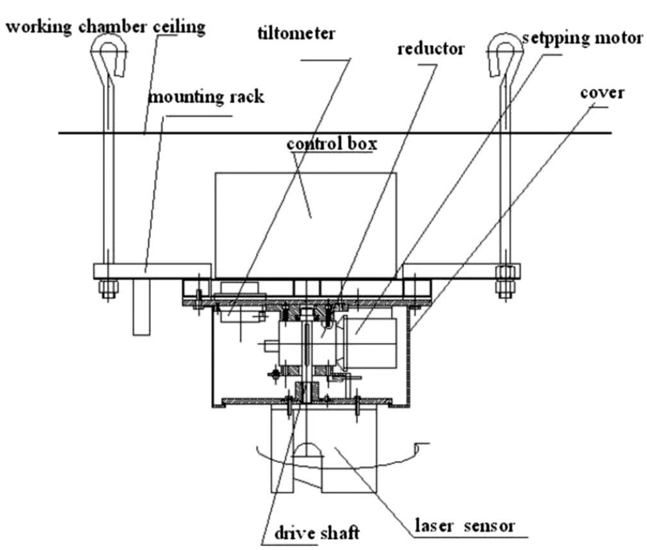

Fig. 4. Schematic diagram of 3D laser scanner for pneumatic caisson

If the sampling point in which a frame scan angle is α, the line scan angle is β (Fig. 3); the distance value is r, which means the coordinate of the point in spherical coordinate is (α,β,r). Then, the coordinate of the point in Cartesian coordinate is calculated as follows:

$$x = r \sin\beta \cos\alpha$$

$$y = r \sin\beta \sin\alpha$$

$$z = r \cos\beta \tag{1}$$

Here, the range of angular α and β is 0–180°; the range of distance is 0–32 m; and the resolution of 2D laser scanner sensor is 10 mm.

Fig. 5. 3D laser scanner installed in pneumatic caisson

Fig. 6. Glance of working chamber inside of pneumatic caisson

Registration Method Based on a Modified Hough Transform

As the working chamber is often very large and contains many devices, which may occlude the laser scanning pulses, one 3D laser scanner cannot cover the whole chamber. Usually, multiple scanners are installed in different locations in the working chamber of the pneumatic caisson. In order to obtain a complete range image of the pneumatic caisson, data from multiple scanners have to be transformed to a single common coordinate system via registration. However, aligning point clouds of multiple 3D laser scanners of pneumatic caisson proves to be a difficult problem. Not only because it is impractical to construct a mounting rack in a large pneumatic caisson and to satisfy the precision of installing a laser scanner, but also because 3D laser scanners may need to be recalibrated from time to time due to "drift."

As a fundamental problem in 3D graphic research, registration of 3D-3D sets of point from different views has been studied in depth (Gregor and Whitaker 2001; Liu and Rodrigues 2002; Salvi et al. 2007; Stamos and Leordeanu 2003; Williams et al. 1999). Some examples are the iterative closest point (ICP) algorithms (Besl and McKay 1992; Huber and Hebert 2003) and feature matching methods (Gregor and Whitaker 2001; Stamos and Leordeanu 2003). However, these methods cannot be directly implemented into our system due to the nature of the pneumatic caisson. First of all, the points' sampling density is very low and is no uniform. Second, the points' samplings are high near to the 3D laser. So, it is very difficult to find corresponding pairs of points or lines between two range images. Considering there are at least five man-made planes (four walls and one floorboard), as shown in Fig. 6, it is natural to align the 3D range data along with these planes.

Our main approach can be described as follows: if the object scanned is a plane, then the subsequent range data without taking noise into consideration must be coplanar. Also, most of the state-of-the-art 3D scanning devices scan from one frame to another and the points on a same frame are in the same frame plane. That is, if the object scanned is a plane, then a subsequent range data without considering noise must be colinear (an example is shown Fig. 7). To cluster those points in straight-line segments, using those straight-line segments instead of points as a HT primitive, we can reduce the computational cost efficiently. Our approach to register 3D point clouds consists of several procedures: extracting and fitting straight-line segments between point sets using the least-squares method; using a modified HT to extract planes from straight-line segments and solving for relative pose from several pairs of corresponding planes.

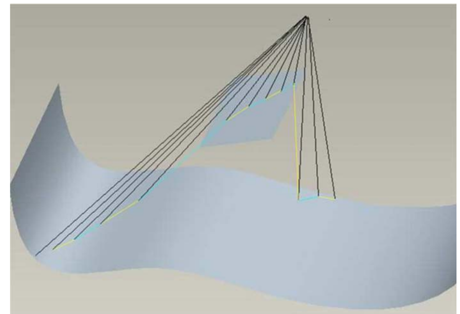

Fig. 7. Concept of fitting straight-line segments

First Procedure—Extracting and Fitting Straight-Line Segments Based on a Least-Squares Method within per Line Scan Frame

The first procedure is to extract straight-line segments from range images so that the planes can be extracted for registration using our modified HT. There are two reasons for using the least-squares method to extract straight-lines segments. First, noise and interference in 3D laser scanner is inevitable. Second, the brick and concrete walls are not homogenous planes. This procedure consists of several steps as follows.

For every line scan frame in each points set, do the following procedure (Fig. 8):

1. Create a new list L to store all points in a straight-line segment. Select the two adjacent points P_1 and P_2 from the line scan frame according to their scan order;
2. If the distance between P_1 and P_2 is less than a distance predefined threshold T_d, we set $L \leftarrow (P_1, P_2)$ and go to Step 3. Otherwise, we pick next point P_3 adjacent to P_2, and set $(P_1, P_2) \leftarrow (P_2, P_3)$, then go to Step 2;
3. Fitting straight line based on a least-squares method, suppose that the list L has n points currently. Let the coefficients of the fitting line be p_n^1 and p_n^2, where n denotes the fitting line has n points and superscript 1 and 2 means the first and second coefficient, respectively. Then the fitting line $y = p_n^1 x + p_n^2$ are computed according to the following equation (Li et al. 2001):

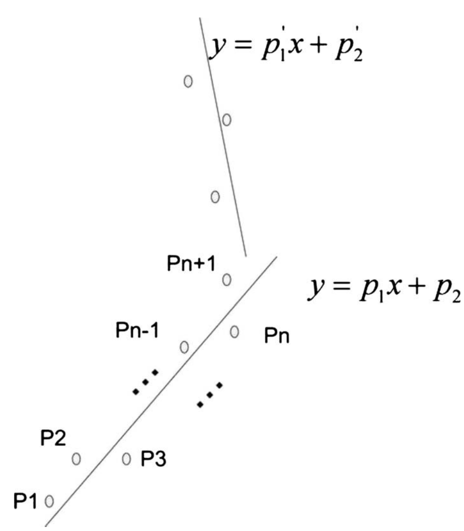

Fig. 8. Schematic diagram of fitting straight-line segments

$$p_n^1 = n\left(\sum_{i=1}^{n} x_i y_i - \sum_{i=1}^{n} x_i \sum_{i=1}^{n} y_i\right) \Bigg/ \left(n\sum_{i=1}^{n} x_i^2 - \left(\sum_{i=1}^{n} x_i\right)^2\right) \quad p_n^2 = \frac{1}{n}\left(\sum_{i=1}^{n} y_i - p_n^1 \sum_{i=1}^{n} x_i\right) \tag{2}$$

where (x_i, y_i)=coordinate of the ith point

$$M_n = \sum_{i=1}^{n} x_i y_i$$

Let $L_n = \Sigma_{i=1}^{n} x_i$, where M_n, L_n, K_n, and H_n denote the sum of n items, respectively

$$K_n = \sum_{i=1}^{n} y_i$$

$$H_n = \sum_{i=1}^{n} x_i^2$$

and rewrite Eq. (2) as

$$p_n^1 = n(M_n - L_n K_n)/(nH_n - (L_n)^2) \quad p_n^2 = \frac{1}{n}(K_n - p_n^1 L_n) \tag{3}$$

Then, if list L has $n+1$ points, we have

$$M_{n+1} = M_n + x_{n+1} y_{n+1}$$

$$L_{n+1} = L_n + x_{n+1}$$

$$K_{n+1} = K_n + y_{n+1}$$

$$H_{n+1} = H_n + x_{n+1}^2 \tag{4}$$

Then, foundation (2) with $n+1$ points in list L can be rewritten as

$$p_{n+1}^1 = (n+1)(M_{n+1} - L_{n+1} K_{n+1})/((n+1)H_{n+1} - (L_{n+1})^2) \quad p_{n+1}^2 = \frac{1}{n+1}(K_{n+1} - p_{n+1}^1 L_{n+1}) \tag{5}$$

4. Pick a point P_1 adjacent to the last point in list L from the scan line, if the distance from point P_1 to the fitting straight line is less than predefined threshold T_l then add P_1 to set L and go to Step 3. Otherwise pick next point P_2, if the distance from P_2 to L is less than predefined threshold T_l, then remove point P_1 as noise and add P_2 to set L and go to Step 3; and
5. If the number of points in list L exceeds the number predefined threshold T_n, convert the line equation from 2D space into 3D space according to its fitting line equation and its location, then add L into line segments list collect LS, go to Step 1; or else remove all points in L and add point P_1 and P_2 to list L and go to Step 2.

Second Procedure—Extracting Planes Based on a Modified Hough Transform Method

This procedure intends to extract planes from straight-line segments cluster which has been extracted in last procedure. As HT has been proven to be a very robust algorithm to detect simple shape in 2D or 3D space (Cha et al. 2006; Ding et al. 2005). Here, we use a modified HT to extract planes from straight-line clusters. The process consists of computing the normal vectors of planes and their last coefficients d which is the distance from the coordinate origin to those planes.

Detection of Normal Vectors

A plane in 3D space can be parameterized in the form

$$x \cos \alpha + y \cos \beta + z \cos \gamma = d \tag{6}$$

where $\alpha \in [0, \pi]$, $\beta \in [0, \pi]$, and $\gamma \in [0, \pi/2]$ denote the angles between the normal vector plane and three coordinate axes, and

$$\cos^2 \alpha + \cos^2 \beta + \cos^2 \gamma = 1 \tag{7}$$

$\mathbf{n} = (\cos \alpha, y \cos \beta, z \cos \gamma)$=normal vector of plane.

As all points are used in the procedure of the standard HT, it is very time consuming (Ding et al. 2005). However, for our case, we have extracted many line segments from the point set. So, a plane can be extracted from point set using the following modified HT which is based on the standard HT. We describe our modified HT method as follows using an "electoral voting system" as an analogy.

The parameter spaces of α and β are appropriately evenly quantized into P portions, respectively, and the parameter space of d, Q portions: as the parameter space of α and β are $[0, \pi]$, respectively, the ith portion of the parameter spaces of α and β are denoted as α_i and β_i, respectively, and then, $\alpha_i = i^* \pi / P$ and $\beta_i = i^* \pi / P$. Suppose that the admissible span of the parameter d is $[d_0, d_{Q-1}]$ (generally, we can set $d_0=0$, and d_{Q-1} as an estimated value of the maximum distance from origin to the possible plane in point could), then, the jth portion of the parameter space of d is denoted as d_j and $d_j = d_0 + j^*(d_{Q-1} - d_0)/Q$. After quantizing the parameter spaces, we can obtain a three-dimensional array $(\alpha_i, \beta_j, d_k)_{P\times P\times Q}$ in which any cell (α_i, β_j, d_k) located in (i, j, k) determines a potential plane (a "candidate"). Those cells owning the same vales of α_i and β_i can be seen as part of the same "party" denoted as (α_i, β_j) (for each party there is Q candidates) and there are $P \times P$ "parties." We then build a three-dimensional integer array C with $P \times P \times Q$ as an accumulator array for $(\alpha_i, \beta_j, d_k)_{P\times P\times Q}$, and then initialized all the cells of the array C to zero. Any cell of the accumulator array C at (i, j, k) can be seen as a "vote" for the candidate (α_i, β_j, d_k). Suppose that we have extracted M straight-line segments ("groups") from the point set, denoted as $\{(S_m) | m=0, 1, \cdots, M-1\}$. For each pair (α_i, β_j) (each party), for each straight-line segment S_m with n_m points (that means, the "group" S_m has n_m "electorates"), by selecting one endpoint ("representative") of the straight-line segment, the corresponding parameter d_k of the plane can be calculated using Eqs. (6) and (7). If the distance from another endpoint (another representative) of the straight-line segment to the plane is less than the predefined threshold T_p, then the number of the accumulator array C corresponding to (α_i, β_j, d_k) is added a number n_m (that means, each group has two "representatives;" one representative must "elect" one candidate from each party and if another representative accepts the candidate, then the candidate will get all the votes of the group). After considering all the angle pairs

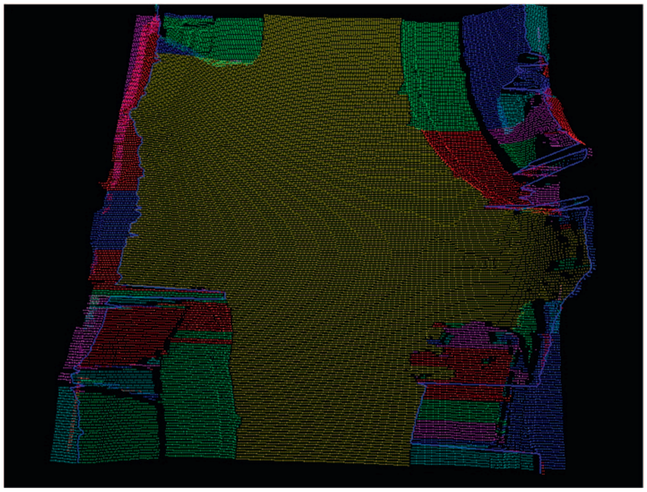

Fig. 9. (Color) Illustration of curves grouping by using spherical parameters

through the entire straight-line segment cluster, a parameter in $(\alpha_i, \beta_j, d_k)_{P\times P\times Q}$ corresponding to the cell with maximum value in the array C is picked up as a probable plane in the point cloud. Considering there must be a wide angle or a long distance between any two planes in a pneumatic caisson, we can search for more planes in the accumulator cell array.

Third Procedure—Solving for Registration Matrix

Here, we reuse the singular value decomposition method presented in the Gregor and Whitaker (2001) paper. Let $n_{1,i}$ and $\omega_{1,i}$ refer to the normal vector and the offset of a plane from a view point, respectively, and from another viewpoint, the normal vector and the offset of the plane are $n_{2,i}$ and $\omega_{2,i}$, respectively. Let R and t refer to rotation matrix and translation vector of rigid transmit, respectively. Then, if a point P lies in a distance d from the plane $\langle n_{1,i}, \omega_{1,i}\rangle$, the point $P'=RP+t$ lies in the same distance form the plane $\langle n_{2,i}, \omega_{2,i}\rangle$. We obtain two plane equations as follows:

$$n_{1,i}^T P + \omega_{1,i} = d \tag{8}$$

$$n_{2,i}^T RP + \omega_{2,i} = d \tag{9}$$

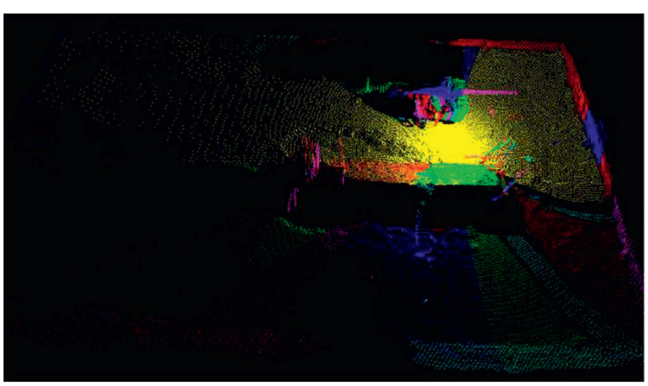

Fig. 10. (Color) Illustration of curves grouping by using Cartesian parameters

After using HT, a number of correspondence planes are given. Let $\mathbf{N_1}$ and $\mathbf{N_2}$ be matrix representations of the two sets of surfaces normal and

$$svd(\mathbf{N_1 N_2}) = \mathbf{U\Lambda V}^T \tag{10}$$

where $\mathbf{U}, \mathbf{\Lambda}, \mathbf{V}$=upper triangular matrix, diagonal matrix, and lower triangular matrix, respectively.

Suppose the registration parameters rotation matrix and translation vector are R and t, respectively. Then, according to the method presented by Gregor and Whitaker (2001), the rotation matrix R is

$$\mathbf{R} = \mathbf{VU}^T \tag{11}$$

and the translation vector $\mathbf{t}$ is

$$\mathbf{t} = \mathbf{V\Lambda}^{-1}\mathbf{UN}_2(\boldsymbol{\omega}_1 - \boldsymbol{\omega}_2) \tag{12}$$

Here, ω_1 and ω_2=vector representations of the two sets of plane offsets.

3D Surface Reconstruction Method

In this paper, the presented reconstruction method is composed of three phases: first to segment point clouds into different regions, then build a triangular mesh and finally evaluate the normal of vertices. In order to rebuild 3D models inside of a pneumatic caisson, such as wall, soil surface, excavators, or even workers, point clouds must first be divided into different regions. Many range image segmentation methods have been published, such as Filin and Pfeifer (2006), which presented a slope adoptive method, and Meyer and Marin (2004), which proposed a method for fitting. But our approach is based on the similarity of the scan curves. The main idea behind our segmentation method is based on the operation mode and the data organization of the 3D laser scanner. As one frame data are composed of a number of scan lines, two adjacent scan lines obtained from the adjacent area of the surface must have some similarities.

After point cloud segmentation, the main steps for surface reconstruction is to build a primitive for surface representation, such as a triangular mesh (Amenta et al. 1998), point (Kobbelt and Botsch 2004; Rusinkiewicz et al. 2002), or other primitives. Triangular meshes are simple, but traditional building mesh methods are too slow to be used in a real-time environment. On the other hand, point-based methods are fast but when the point density is low, the surface may have many gaps and the resulting surface reconstruction will be undesirable. Tubic et al. (2003) presented a surface modeling method from curves. The main idea of the curves method is similar to the point-based methods on approximating surface by small plane patches. As the curves method inherits geometric properties such as normal and location by analyzing curves, this method is more convenient than the point-based method in computing geometry property. But gaps, however, cannot be avoided since the point density is low. Our modeling approach has some similarity with the curve method (Tubic et al. 2003) but we use triangular meshes instead of point-based method in Tubic's method.

Normals are absolutely necessary for rendering or texture mapping in 3D computer graphic. However, the point cloud obtained from our 3D laser scanner only have location and distance information. The normal of the points are thus computed based on their neighboring points. Currently, three kinds of methods are used for evaluating the normal of points. The first method for computing point normal is principal component analysis. If a

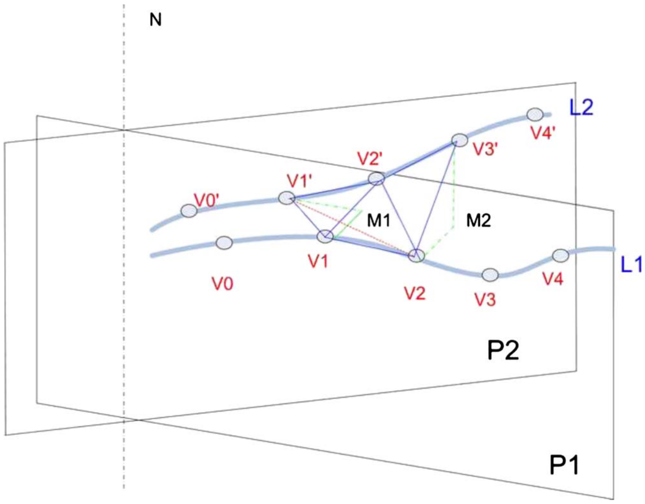

Fig. 11. Illustration of reconstruction from two neighbor curves

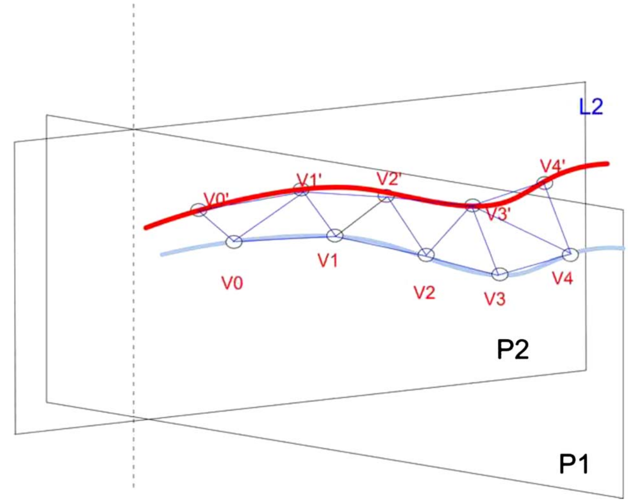

Fig. 13. Illustration of reconstruction from a curve without neighbor curve; the curve L_2 is created by rotating curve L_1 around axis N

point p_i and its neighborhood point set $(p_{i,1}, p_{i,2}, \ldots, p_{i,k})$ are given, then the covariance matrix C of the point p_i about its neighborhood points can be defined as

$$C = \sum_{j=1}^{j=k} (p_j - \bar{p})(p_j - \bar{p})^T \in IR^{3\times 3} \tag{13}$$

Here

$$\bar{p} = \frac{1}{k}\sum_{j=1}^{k} p_j$$

Evaluating the eigenvalues and eigenvectors of the covariance matrix C, the eigenvector corresponding to the minimum eigenvalue is the normal of the point p_i. The second method for computing point normal is the method of fitting. If a point p_i and its neighborhood point set $(p_{i,1}, p_{i,2}, \ldots, p_{i,k})$ are given, then a plane can be obtained by the fitting method, the normal of the plane are regarded as the normal of the point. The last method is a moving least-squares method (MLS). In MLS, a hyperplane is computed and the normal of the hyperplane is regarded as the normal of the points.

In this paper, the normals of vertexes are evaluated by using the neighborhood triangular mesh of the vertex. The reason for this is that the point density is not uniform and the triangular meshes have been built before computing the normal of the vertexes. The following are the detailed descriptions of the three phases for 3D reconstruction of a pneumatic caisson—segmentation, reconstruction, and evaluation of the normals of the vertexes.

First Phase—Segmentation and Region Merge Based on Curves in Local Scanner Coordinates

During the first phase, we first partition each scan line into different curve segments, which is partially similar to University of Berne (UB) methods (Jiang and Bunke 1999), but our method has two main differences. First, we partition scan lines in their

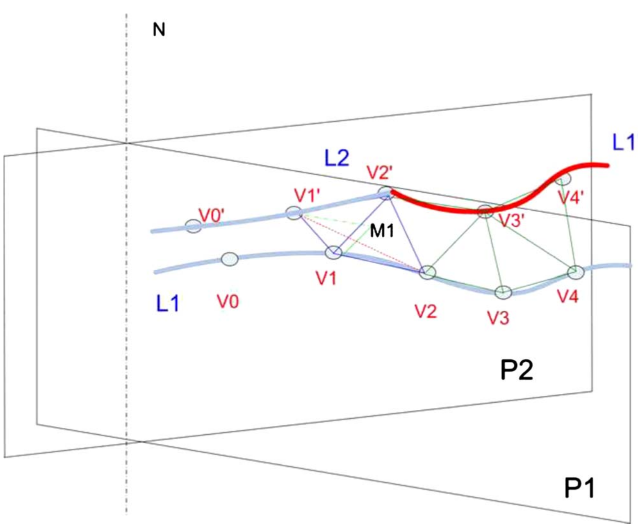

Fig. 12. Illustration of reconstruction from a curve at which some points have no the nearest points; the curve segment V_2V_4 is created by rotating the correspondence points around the axis N

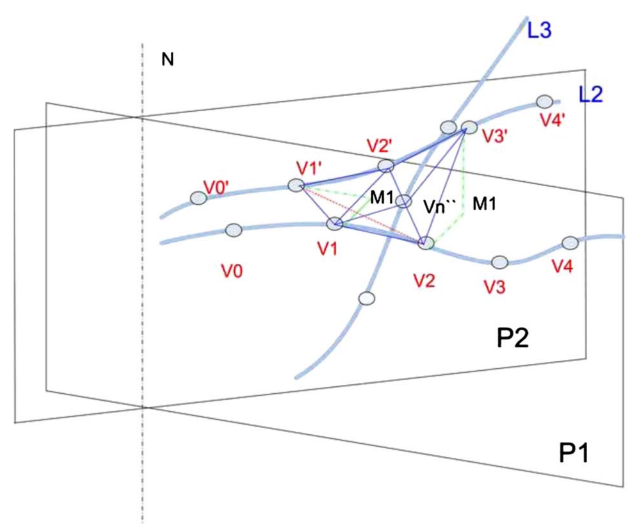

Fig. 14. Illustration of reconstruction from curves obtained from different laser scanners

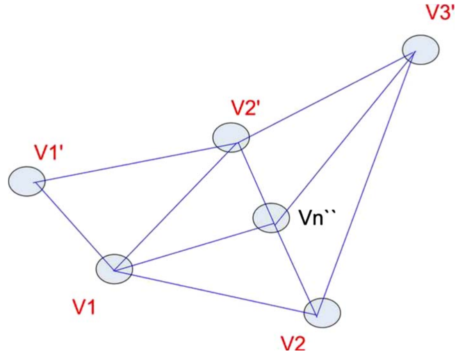

Fig. 15. Normal of V' is $n=n'/|n'|$

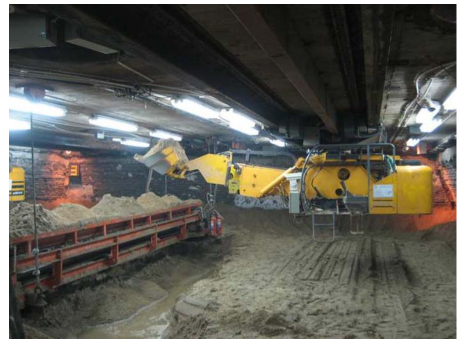

Fig. 16. Glance of the working chamber inside of the pneumatic caisson during excavating

local coordinate by using spherical parameters of scan lines. Second, we use statistical methods instead of geometry methods. And then we evaluate the statistical variant of each curve segment. Last, we perform a region-growing algorithm according to their similarities.

Partitioning Scan Lines into Curve Segments

Points collected from a single 3D laser scanner are organized by spherical parameters (α,β,r) in the local coordinate of the laser scanner. The main reason for using spherical parameters as segmentation media is that data structures of the points from a single 3D laser is regularly organized according to the running path of the laser scanner and thus the range image using spherical parameters will be easy to preprocess using general image processing methods. Fig. 9 shows the same range image in spherical parameters and Fig. 10 shows a range image collected from a local 3D scanner using Cartesian coordinate parameters.

As the surfaces of the scanned objects, such as ground surface and walls, are not smooth and regular but irregular and fractal, the common partitioning 3D methods are invalid. We split the scan lines by computing the following parameters according to the following lemmas.

The maximum value at each scans line or curve

$$M_i = \max[r_{i,j}(\alpha_i,\beta_j)], \quad i=0,\cdots,n$$

$$j=0,\cdots,m \tag{14}$$

where M_i=maximum of $r_{i,j}$ at the ith scan line.

The differential value of two neighbor points

$$\Delta D_{i,j} = r_{i,j} - r_{i,j-1}$$

$$i=0,\cdots,n$$

$$j=1,\cdots,m \tag{15}$$

Quadric difference of two neighbor points

$$\Delta^2 D_{i,j} = \Delta D_{i,j} - \Delta D_{i,j-1}, \quad i=0,\cdots,n$$

$$j=2,\cdots,m$$

For each scan line, the partition process has several steps described as follows:

- Step 1, if the point with the maximum value is not endpoint, split the scan line into two curves at the maximum point;
- Step 2, if the differential value of two neighbor points is over the threshold T_{D1} predefined, then split the curve into two parts at the point;
- Step 3, if the quadric difference of two neighbor points is over the threshold T_{D2} predefined, then split the curve into two parts at the point; and
- Step 4, after segmenting all scans lines, curves set are obtained, where all points in a curve may belong to the same object.

Curves Grouping Based on the Similarity of Curves Segments

Curves grouping come from the simple idea that if the points of two neighboring curves are collected from same object, they must have some similarity. We compute the similarity of two curves by using statistical variables which are described as follows.

Given a curve with n points, mean value of the curve is defined as

$$E_i = 1/k\sum_{l=1}^{l=k} r_{i,j_l}, \quad l=(1,\cdots,k) \tag{16}$$

where k denotes the number of points selected from the curve at a corresponding location and r_{i,j_l}=distance from the point to the laser scanner. Then we compute the distance of the two mean values of the two neighbor curves, if their distance is less than the threshold T_{dis} predefined then two curves are classified into one class, otherwise, classified into the two different classes.

Region Growing Based on the Similarity of the Small Region

We first group curves into small regions then group small regions into large, the reason lies in that the relation between splitting scan lines into curves and curves grouping is an inconsistency. If scan lines were split into too many short curves, regions obtained may be small, but obtained more probably from one object. If scan lines were split into few long curves, region obtained may be large, but from different objects. The presented region growing has three steps. First, mean values of the points at small region border are computed according to the aforementioned foundation. Then, we compute the distance values of the small region com-

Table 1. Registration Parameters

T_d	T_l	T_n	P	Q	D_{Q-1}	T_p
20	6	8	200	400	3,200	12

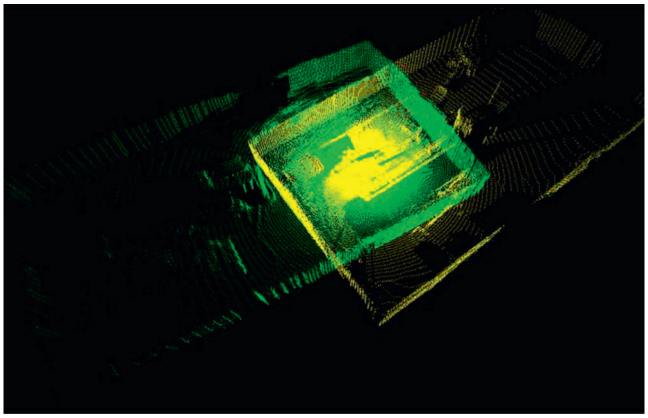

Fig. 17. (Color) Two range images without registration

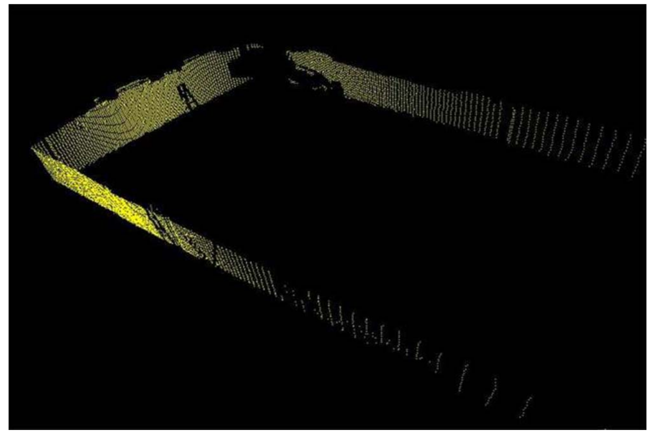

Fig. 19. Other four planes

paring with its neighbor regions. Third, a nearest neighbor region is found in its all neighbor regions, and if the distance value of the two regions is lower than the threshold predefined, then the two regions are merged into one region.

Second Phase—Build Triangular Mesh

In order to reconstruct the model in real time, by taking advantage of the special properties of the data in the curves set obtained by the aforementioned methods, we present a simple method to build triangular meshes in this section. Our method is different with the traditional building triangular mesh methods, such as Voronoi-based methods (Amenta et al. 1998), Delaunay-based methods (Schall and Samozino 2005), which are very time consuming and unfit for reconstruction of a pneumatic caisson.

Our method is described as follows. For each curve L_1 on a scan plane P_1 find out if there is a neighbor curve at the neighbor scan plane P_2.

1. Picking up points
   a. If L_1 has a neighbor curve L_2 at the neighbor scan plane P_2, pick up two neighbor points (master points) along given a direction at the curve L_1 (V_1, V_2 at curve L_1 in Fig. 11), then find the nearest points of the two master points at its neighbor plane P_2 (V_1' and V_3' at the curve L_2 in Fig. 11);
   b. If the nearest points are both at the neighbor curve, then pick up all points between the two nearest points as a group points, those points including the two nearest points are called slave points (Fig. 11);
   c. If only one or none of the nearest points of the two master points are at the neighbor curve then rotate the point without the nearest point around the axis N with degree φ which is the angle between two neighbor planes. The new points created are called mirror points (such as the points in the red curve in Fig. 12); and
   d. If L_1 has no neighbor curve, then create a new curve by rotating L_1 around the axis N with degree φ which is the angle between two neighboring planes (such as those points in the red curve in Fig. 13).
2. Building triangles. Two master points with its slave points or mirror points are used to form a group of triangles according to the principle described as follows:
   a. If there are four points (two master points, two slave points or mirror points) which form a quadrangle in R^3 space; compare the two diagonal lines; select the shorter diagonal line as a common edge of the two triangles; and
   b. If there are more than four points, pick up first two slave points or mirror points along the predefined direction as well as two master points form a quadrangle in R^3 space. Then, build two triangles according to the description earlier (such as $\triangle V_1V_2'V_1'$ and $\triangle V_1V_2V_2'$ in Fig. 11). As to the rest of slave points or mirror points

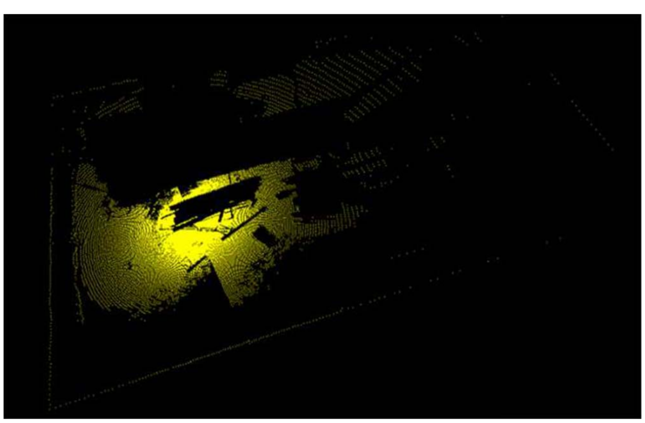

Fig. 18. Plane with maximum points

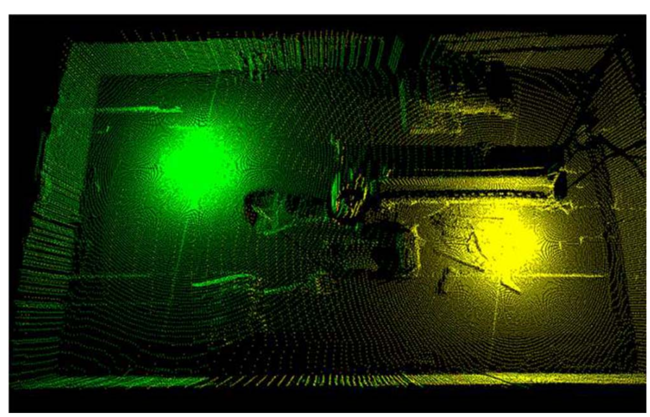

Fig. 20. Result of registration

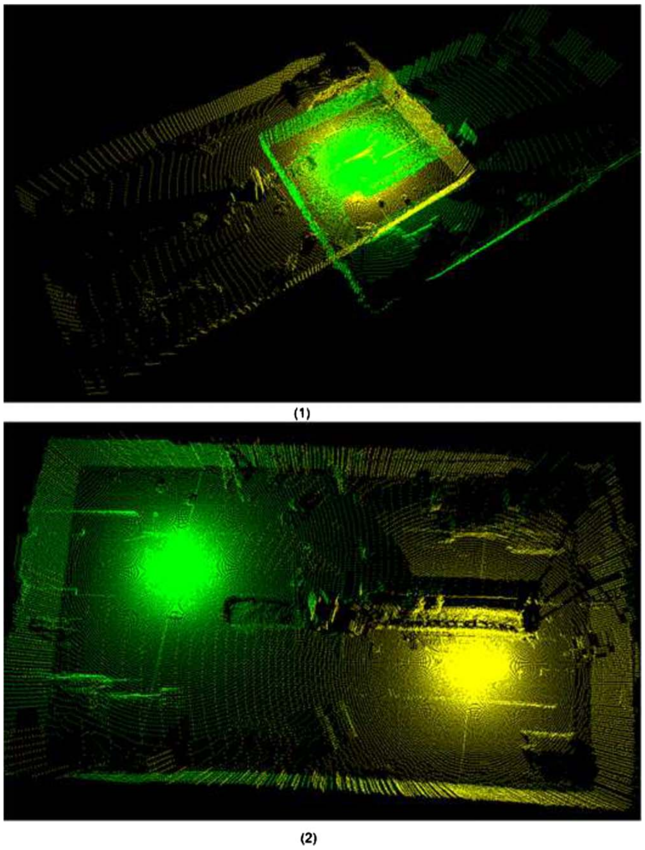

Fig. 21. Test for registration: (1) two point sets without registration; (2) the result after registration

can form a set of triangles fan with the last master point ($\triangle V_2V_3'V_2'$ in Fig. 11).

3. Processing points obtained from another laser. In this step, we need to find out whether points obtained by other laser scanners are within the bound of the triangles built according to the preceding step. If the point falls in the bound of the quadrangle, we divide it into four triangles (such as, in Fig. 14, V_n'' at L_3 which obtained from other laser scanner). If the point falls in the bound of a triangle we divide the triangle into three triangles; and
4. Go to Step 1 until all points at the curve have been processed.

Third Phase—Evaluate the Normal of the Point

The first step in computing the normal of a point V is obtaining cross products of the two vectors of triangles which contain the point V. If given a triangle with vertex points V, V_i, V_{i+1}, then the cross product is

$$\mathbf{n}_i = (\mathbf{V} - \mathbf{V}_i) \times (\mathbf{V} - \mathbf{V}_{i+1}) \tag{17}$$

and the normal n of the point V is

$$\mathbf{n} = \sum_{i=1}^{k} \mathbf{n}_i \Big/ \left| \sum_{i=1}^{k} \mathbf{n}_i \right| \tag{18}$$

where k means there are k triangles that contain vertex V. The foundation means that the normal of a point are determined by the areas of the triangles which contain the point. As an example is shown in Fig. 15, if

Table 2. Segmentation Parameters

T_{D1}	T_{D2}	T_{dis1}	T_{dis2}
70	40	20	40

$$\mathbf{n}' = (\mathbf{V}_n' - \mathbf{V}_1) \times (\mathbf{V}_n' - \mathbf{V}_2) + (\mathbf{V}_n' - \mathbf{V}_2) \times (\mathbf{V}_n' - \mathbf{V}_3') + (\mathbf{V}_n' - \mathbf{V}_3') \times (\mathbf{V}_n' - \mathbf{V}_2') + (\mathbf{V}_n' - \mathbf{V}_2') \times (\mathbf{V}_n' - \mathbf{V}_1)$$

Then the normal of V_n' is $\mathbf{n} = \mathbf{n}'/|\mathbf{n}'|$.

Discussion and Analysis of Result

Overview

The 3D surface modeling and measurement system described in 3D Surface Modeling and Measuring System for Pneumatic Caisson has been implemented on a pneumatic caisson in a subway construction site in Shanghai, China. The pneumatic caisson is an air pit between two subway stations which is 25 m long, 12 m wide, and its final depth is 29 m (Fig. 16) and the relative pressure inside it is less than 0.4 Mpa. According to the volume of the pneumatic caisson, we built two 3D laser scanners. Considering the different needs between managers (or researchers) and excavation operators, in this practical application a client/server architecture (two PCs with P4 2.8 GHz and independent graphics card) were used, one the server PC with lower reconstruction performance but faster rendering speed was used for excavator operators and client PC with higher reconstruction performance but slower rendering speed was used for managers and researchers. All data from the sensors (two 3D laser scanners, two distance laser sensors, and one inclination sensor) inside the pneumatic caisson are transmitted to the server first, and then the client reads the data from the server. The algorithms for registration and segmentation used in the two PCs are the same. There are only some minor differences in their reconstruction methods. The software on both PCs is built using VC++ 6.0 and OpenGL.

3D Laser Scanner

As the whole system must operate in an extreme environment of the pneumatic caisson, the proper selection of the sensors used has an important influence on the performance of the system. We selected the SICK LMS-290 as our laser scanner. In this application, without considering occlusion, the design prerequisite for point density is 20 cm, which means that 3D laser scanners is able to sample at least one point within a 20×20 cm^2 area. According to the requirement for point density and the volume of the pneumatic caisson, in our case, we selected 0.5° angular resolution of the laser sensor and selected 200 lines in one work cycle, which means if the laser sensor was rotated 180° in a uniform circular motion around its rotated axis by step motor, then 200 scan lines would be passed into the pneumatic caisson space. The speeds of the stepping motor are mainly determined by how many scan lines are needed to pass the entire space. Fig. 10 shows the point cloud obtained from one laser scan and Fig. 21 shows the common point cloud obtained from two laser scans, both of them are obtained from one work cycle. Figs. 22(1, 2, and 3) show the raw data after registration. The performance of the 3D laser scanner was tested using two methods; the first method is by observation. By comparing the 3D image (point cloud) with the geometric appearance of the object inside the pneumatic caisson,

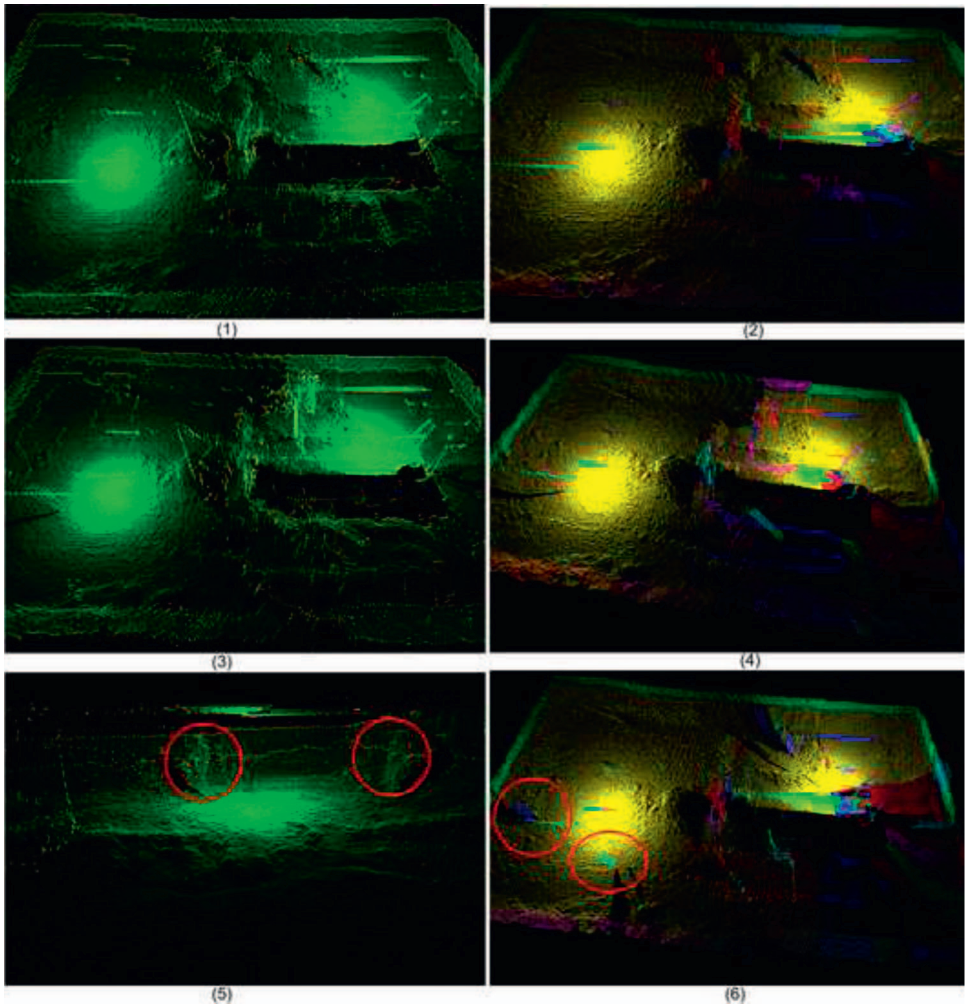

Fig. 22. (Color) Illustration of partition and curve grouping: (1) and (2) are the same training sample for the second case: (1) raw data after partition; (2) curve grouping. (3) and (4) are the same training sample from the third case: (3) raw data after partition; (4) curve grouping. (5) and (6) are the same training sample from the fourth case: (5) raw data after partition; (6) curve grouping. Note: the bigger yellow points in (1), (3), and (5) are the segmentation points and the location of maintenance workers are denoted by the red circles.

we can determine if there were distortions with the 3D image. The observation method is very important in our application and experiment. In fact, observations of the 3D images collected were qualified manually throughout the whole process of the project. For example, by comparing Fig. 6 with Fig. 20 and comparing Figs. 10 and 21 with Fig. 16, the 3D images display the belt conveyer, excavators, and other objects well and without distortion. The second method is using measurement. We use this method to measure the work cycle and the resolution of the 3D laser scanner because during our tests, we found that the rapid fluctuation of air pressure inside of the pneumatic caisson had an effect on the speed and resolution of the SICK laser scanner sensor. Especially, when the pressure falls sharply, the scanning speed of laser scanner will slow down as compared to operations under normal conditions. For this reason, the work cycle of the 3D scanner is not constant and is determined by the operating conditions. To measure the two parameters, we performed a simple experiment during the first aeration test. We placed the 3D laser scanner into the pneumatic caisson. We then set a timer in our computer program and recorded the average work cycle of our 3D laser scanner. The average time recorded for the 3D laser scanner to complete a work cycle was less than 16 s. Resolution, another important parameter that indicates the performance of a laser sensor, relates to the minimum variation of distance that can be detected by a laser sensor. In order to measure the minimum resolution of the laser scanner under the aforementioned pressure fluctuations, we obtained a ground truth by placing a small work table of known dimensions into the pneumatic caisson and compared the measured values of the laser scanner. The result shows that the estimated resolution is less than 20 mm.

Registration

The registration experiment was carried out mainly before the floorboard was ruined and the experiment mainly involves predefining seven parameters. In order to extract such a "good" plane from each point set that it can approximate the floor well, we selected a sample point cloud which was obtained when both excavators were stopping work and there were little miscellaneous on the floor. In order to validate the registration result, we select a sample randomly. The first three parameters (T_d, T_l, T_n) are for fitting method and the other parameters (P, Q, d_{Q-1}, T_p) are for HT (Table 1). The distance predefined threshold T_d, which means that if the distance between two points were beyond T_d, these two points must not lie in one straight-line segment. In general this parameter can be determined according to the design

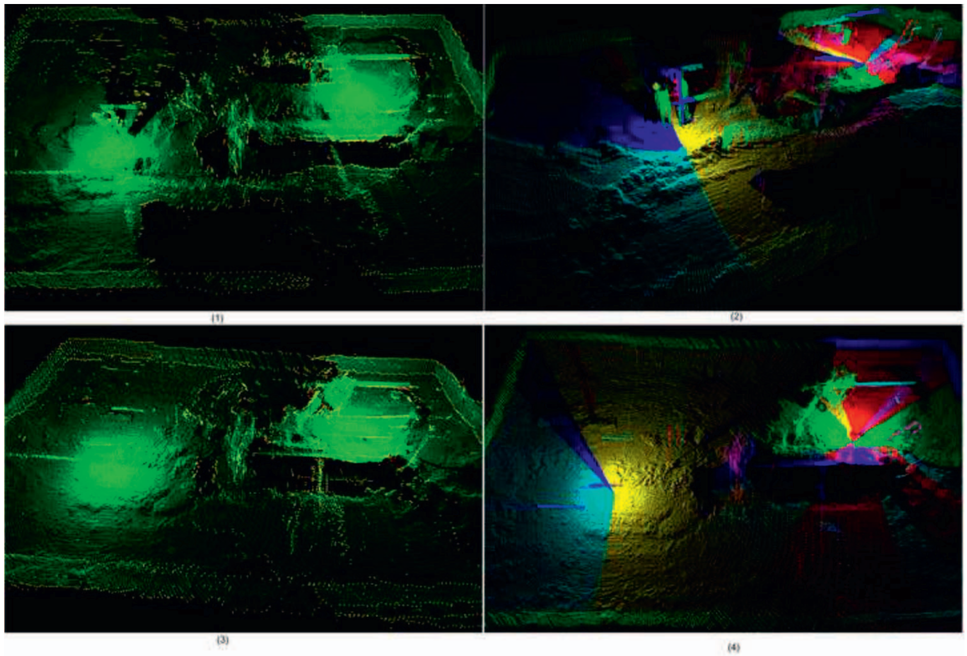

Fig. 23. (Color) Illustration of partition and curve grouping: (1) and (2) are the same testing sample: (1) raw data after partition; (2) curve grouping. (3) and (4) are the same testing sample: (3) raw data after partition; (4) curve grouping. Note: the bigger yellow points in (1) and (3) are the segmentation points.

value of point density, in our case, T_d was set at 20. The parameter T_l means if the distance from a point to a fitting line is beyond T_l, then the point must not lie in the fitting line. This parameter determines the maximum length of a fitting line; we manually adjust the parameter according the length of the fitting line and T_l was set at 6. The threshold T_n means that if a list have more points than T_n, then the list can be regarded as a straight-line segment. The setting of the parameter also depends on manual adjustment. In our experiment, we set T_n as 8. As for the parameters of HT, because there are 200 scan lines in one work cycle and 361 points at one scan line, P was set as 200 and Q was 400. As the maximum measurement distance of the laser sensor is 32 m, we set d_{Q-1} as 32,000. The function of T_p is similar to T_l, but we set T_p as 12. Currently, evaluating the performance of a reg-

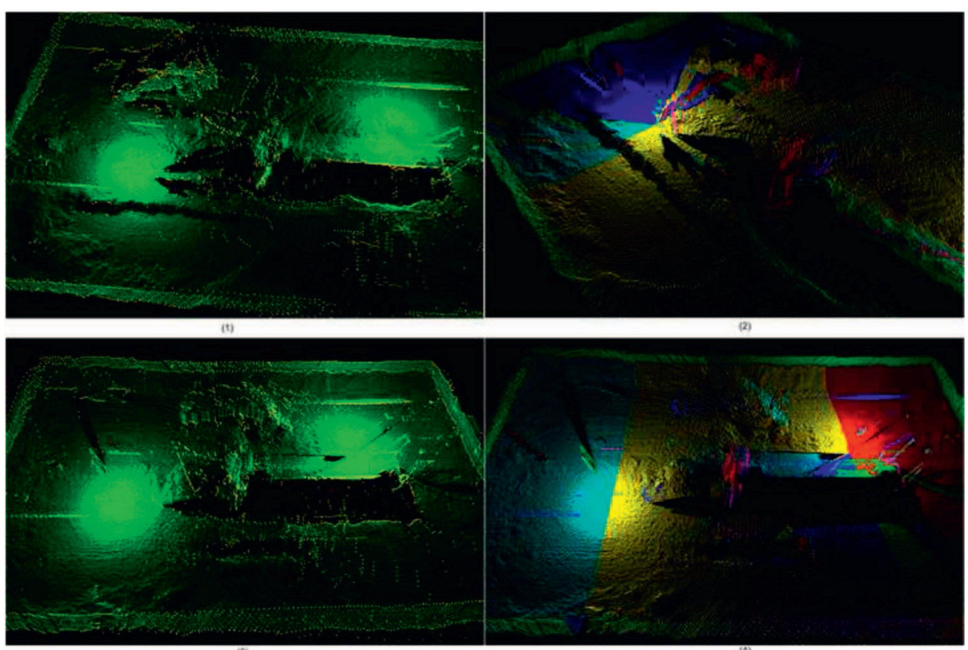

Fig. 24. (Color) Illustration of partition and curve grouping: (1) and (2) are the same testing sample: (1) raw data after partition; (2) curve grouping. (3) and (4) are the same testing sample: (3) raw data after partition; (4) curve grouping. Note: the bigger yellow points in (1) and (3) are the segmentation points.

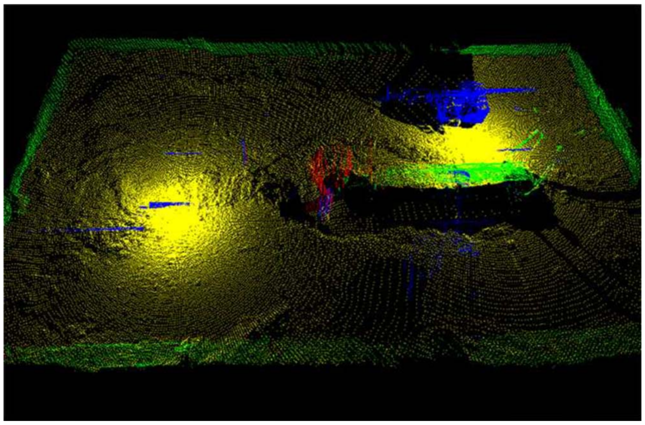

Fig. 25. Illustration of region growing of the training sample for the first case

istration method is still a difficult problem (Salvi et al. 2007; Stamos and Leordeanu 2003). We can evaluate our registration method through manual observation. Fig. 17 shows the point clouds without registration are obtained from the two 3D laser scanners. After extraction plane via our modified HT, five planes shown in Figs. 18 and 19 are extracted. By observing the two figures, the result can be seen as five good planes. Fig. 20 shows the registration result of the training sample. Fig. 21(1) shows the point cloud without registration. Fig. 21(2) shows the registration result for the test sample using the same registration data as the training sample. Both Figs. 20 and 21(2) show that those points (in green) obtained from one 3D laser scanner, in which the four walls and excavators, are well within alignment with that obtained from another 3D laser scanner (in yellow).

Segmentation

Segmentation is a critical step, which has a strong influence on the quality of the 3D reconstruction. In this application, segmentation includes two steps (partition and merge). As several parameters need to be predefined and the real application is very complicated, we classified our application into four cases. The first case is that both excavators were stopping work. The second case is on that excavators were moving. The third case is on that

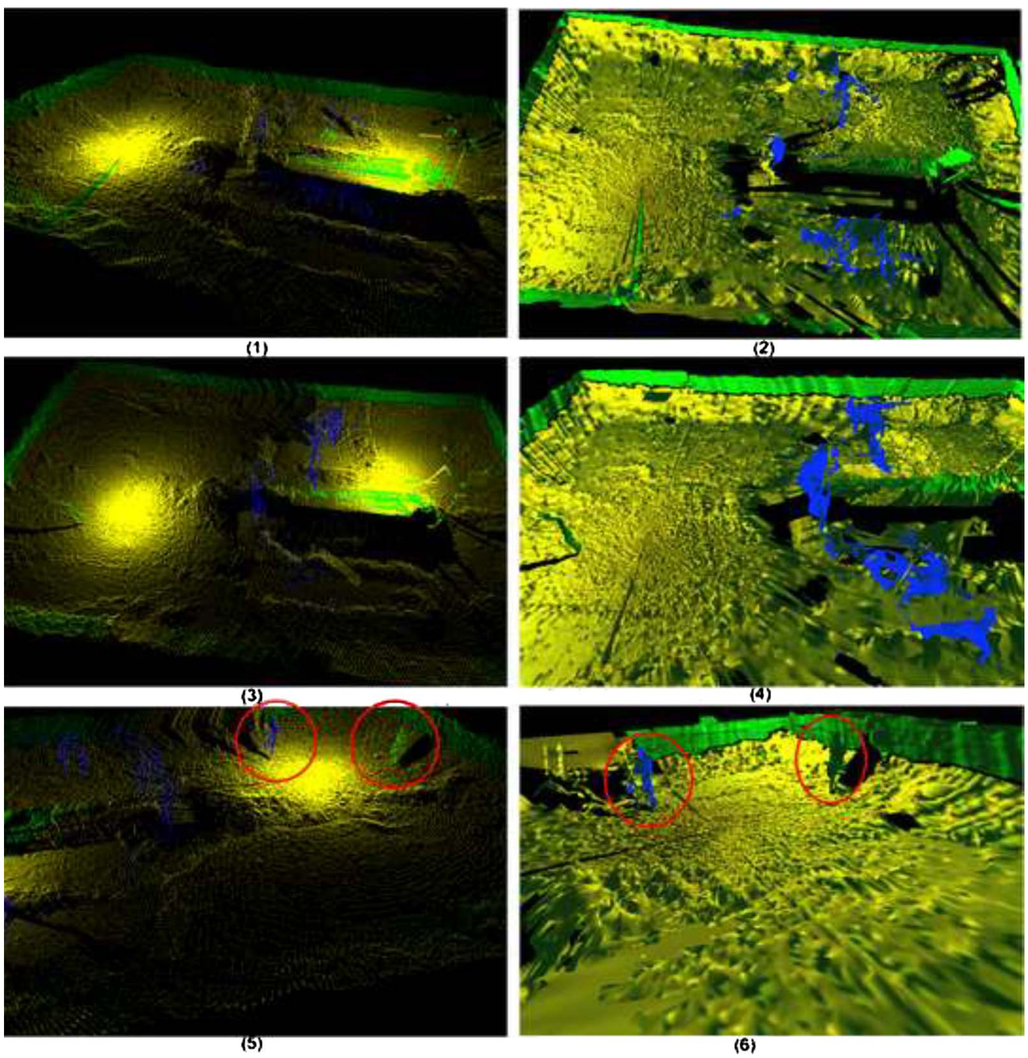

Fig. 26. Illustration of region growing and reconstruction for the three training samples: (1) and (2) are a sample of the second case: (1) region growing; (2) reconstruction. (3) and (4) are a sample of the second case: (3) region growing; (4) reconstruction. (5) and (6) are a sample of the second case: (5) raw data; (6) reconstruction. Note: the location of maintenance workers are denoted by the circles.

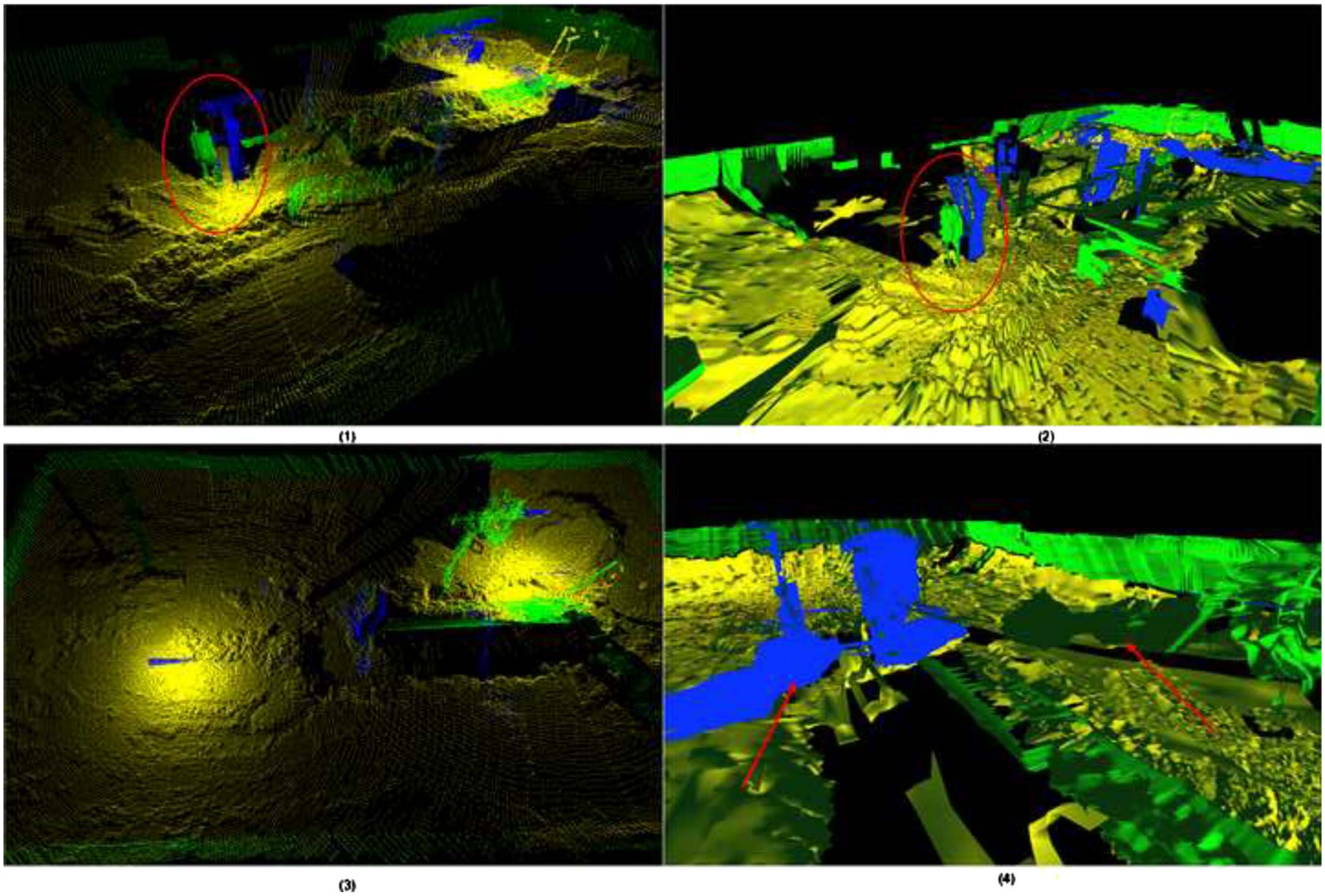

Fig. 27. Illustration of region growing and reconstruction: (1) and (2) are from the same test sample: (1) region growing; (2) reconstruction. (3) and (4) are from the same test sample: (3) region growing; (4) reconstruction. Note: the location of maintenance workers are denoted by the circles.

excavators were digging. The last case is on that maintenance workers were inside the working chamber. In order to determine the parameters, we selected four samples from the preceding four cases, respectively, as training data. However, generally, we pay more attention to the first case because it is a stable and the pneumatic caisson most of the time is in it. For this reason, we determined the parameters first, considering the first case and then refine the parameters using the rest of the three cases. Training parameters involves three steps. The first is to train and test the two parameters for the scan line partition, and then to train and test the parameter for the curve grouping, and finally to train and test the parameter for region growing. In order to test the parameters obtained, 16 test samples were selected randomly from the four cases.

Partition needs two predefined thresholds for $\Delta D_{i,j}$ and $\Delta^2 D_{i,j}$ (Table 2); the first threshold is used to decide if occlusion is between two neighboring points. In our case, we set this parameter as 70, manually. The second parameter is mainly used to differentiate between the conveyer belt and the ground surface. We set this parameter as 40 manually. The key factor in the differentiation problem in this application is to differentiate between the ground surface and the walls. In this application, we use the maximum value method to differentiate between ground surface and walls. The fold lines in Fig. 9 is the dividing line between ground surface and walls and the points in the lines are all maximum values. As shown in Fig. 9, the maximum value method can divide ground surface and walls very well. The reason for this can be simply described as follows. Suppose that the partition of a scan line located in the wall and ground surface can be approximated by two line segments, the distance value r [see Eq. (1)] of the intersecting point is more than that of any points at the curve. It is also for the same reason that spherical parameters are used for segmentation in this application. Figs. 22(1, 3, and 5) show the partition results for the training samples in which the bigger points in yellow are the segmentation points. The testing sample results are similar to the training samples. Figs. 23(1 and 3) and 24(1 and 3) show four testing samples. By manual inspection, the borders of excavators, the belt conveyer, and other objects are clearly segmented.

The parameter for grouping curves is very critical; we select two points from both the end of the curves. That means there are two mean values for one curve respectively. After the parameters for partition were set, we use the same four samples to train the predefined threshold pre for T_{dis1} (Table 2). According to the design value of point density, we set the predefined threshold in this procedure as 20. Figs. 9 and 10 present an example of curves growing for the training sample of the first case. Fig. 9 is presented using spherical parameter and Fig. 10 is shown with Cartesian parameters, in which different regions are shown with different colors. The other three training examples for the rest of the three cases are shown in Fig. 22. The raw point sets are shown in the left column of Fig. 22 and the results of the curve

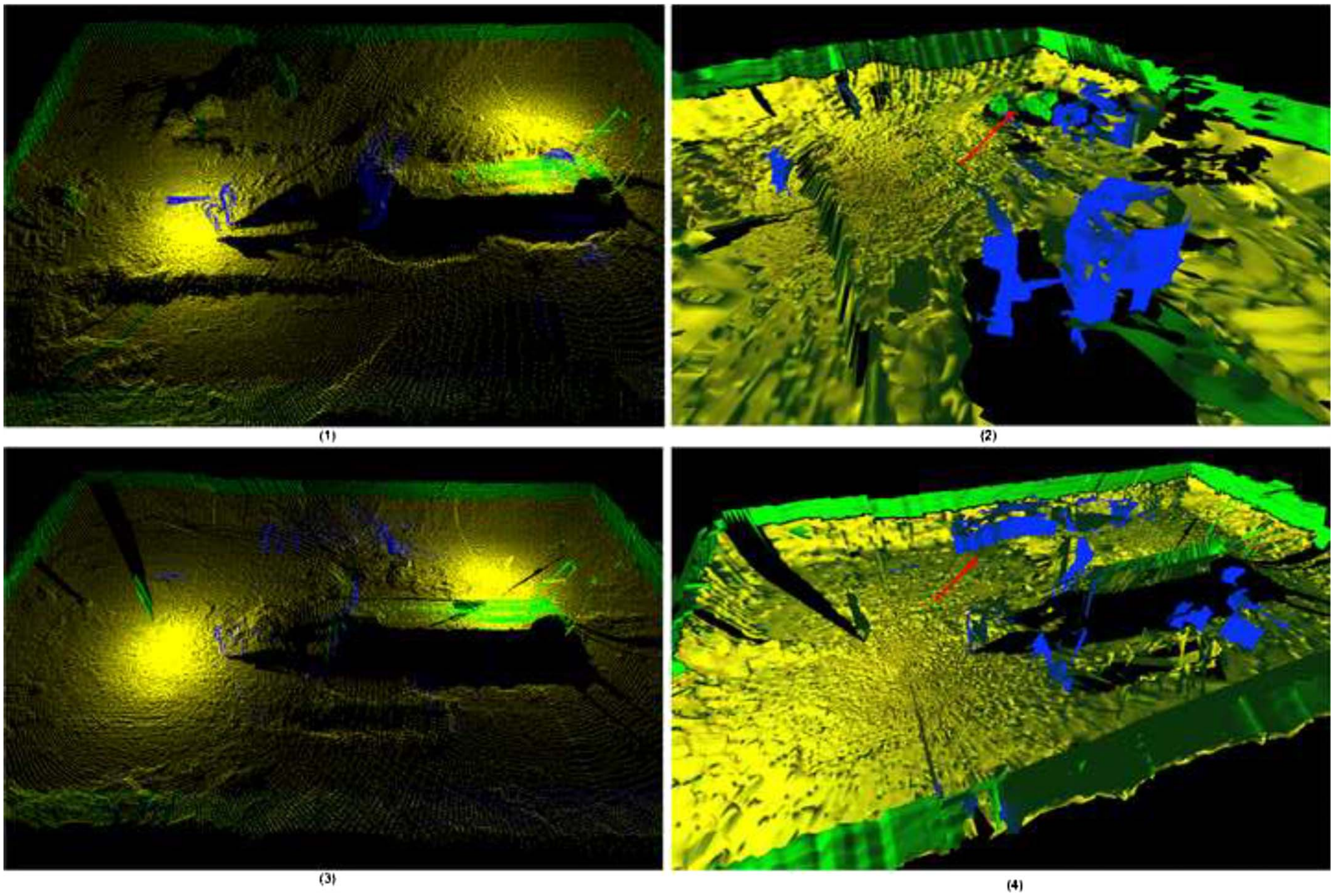

Fig. 28. Illustration of region growing and reconstruction: (1) and (2) are from the same test sample: (1) region growing; (2) reconstruction, the red row indicates a digging excavator. (3) and (4) are from the same test sample: (3) region growing; (4) reconstruction, the red row indicates a slowly moving excavator.

grouping are shown in the right column. From the first two rows in Fig. 22, excavators appeared more blurry than it did in Fig. 10. And from the last row in Fig. 22, the points obtained from maintenance workers can be grouped into two regions well. The results of the testing samples are similar to the training samples. Figs. 23(2 and 3) and 24(2 and 4) show the curve grouping results of four test samples. By manual inspection, the results show that the points from the excavators, surface, walls and even the maintenance workers can be grouped into the same region, respectively.

Region growing is similar to curves grouping; the only difference is that we set the predefined threshold T_{dis2} as 40 (Table 2). An example of the first case is shown in Fig. 25. By comparing the result of segmentation with the scene inside the pneumatic (Fig. 16), the boundaries of ground surface, walls, excavator, and other objects are visually distinct. Figs. 26(1, 3, and 5) show the region growing result for the samples from the rest of the three cases. The testing sample results are similar to the training samples. Figs. 27(1 and 3) and 28(1 and 3) show the region-growing result for the four testing samples.

Reconstruction

The reconstruction involves two parameters(N axis and φ), in this application N is Z axis and φ is 0.9° (180°/200, in one work cycle there are 200 scan lines). In order to do the 3D reconstruction well for the managers and the researchers, 3D surface reconstruction on the client PC is done with almost all the obtained points, since point density is low. Fig. 29 shows the result of 3D reconstruction of the training sample from the fist case, which presents a well appearance, especially on the ground surface and walls. In the right column of Fig. 26, the examples of reconstruction are shown for the rest of the three training samples. Figs. 27(2 and 4) and 28(2 and 4) show four reconstruction results of the testing samples. During excavation construction, the excavation specification does not allow excavation operators to excavate the deep pit. Managers and researchers made and checked the construction progress by observing the appearance of the ground surface and measuring some points on the client PC. During subsidence of the pneumatic caisson, managers and researchers first observe the ground surface inside the pneumatic caisson, then, they select some "suspicious" areas, and then flag them on the areas in the client PC. In the whole subsidence process, they generally measured those areas many times and compared the results. Fig. 30 also gives an example reconstruction with triangles and measurement.

On the server PC, excavators, conveyer belt, and drum are built according to their shapes and the walls are not presented as they may block the line of sight. Because the speed of the excavators can reach very high speeds, rendering speed on the server PC also needs to be fast. Furthermore, there are 10 monitoring

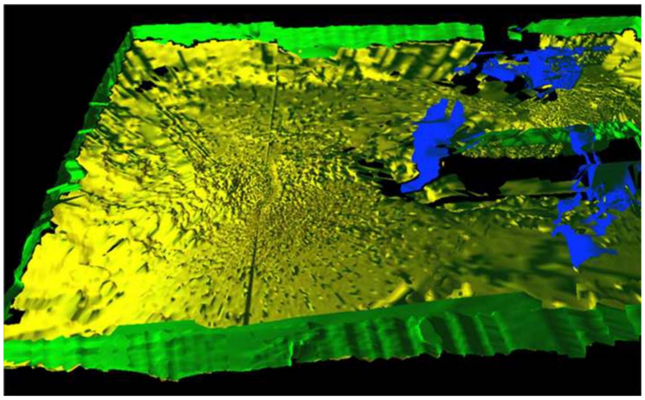

Fig. 29. Illustration of 3D reconstruction of pneumatic caisson

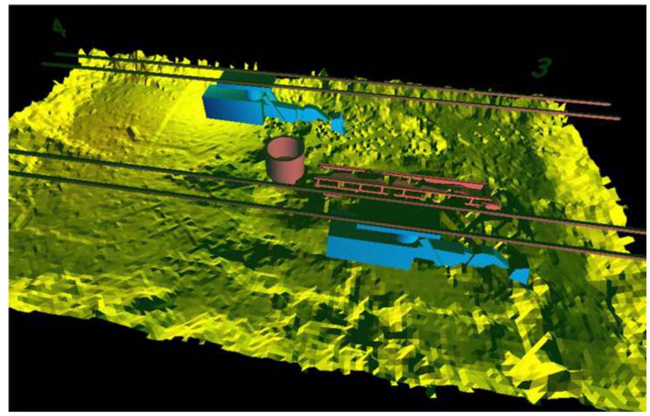

Fig. 31. Illustration of importing models into the 3D environment

display in the control room and excavation operators more concerned with where their excavators are. For those reasons, we can reduce the number of triangles calculated on the server PC. Fig. 31 shows an example of the reconstruction with importing models.

Conclusions

This paper presents a 3D laser scanner system for a pneumatic caisson with many sensors. The 3D laser scanner system can scan the overall space of the pneumatic caisson; and that data are registered to the excavator's pose and location. The paper presents a registration method based on HT which lowers the cost of installing a commercial 3D laser scanner dramatically. Another main contribution is segmentation and reconstruction of the 3D model from curves. As for segmentation, we divided a scan line into several curves according to the point's property, and then, we merge the curves into regions according to the curves' properties. As for the 3D surface reconstruction, we also emphasize using the information contained in curves. The system has been used in a practical pneumatic caisson during the whole construction period. The result shows that the system can satisfy the demand for speed and resolution during data acquisition. The result also shows the system can bear the environmental impacts such as high air pressure, high temperature, and humidity. The result also shows the segmentation algorithm and 3D surface reconstruction method can be used in real time.

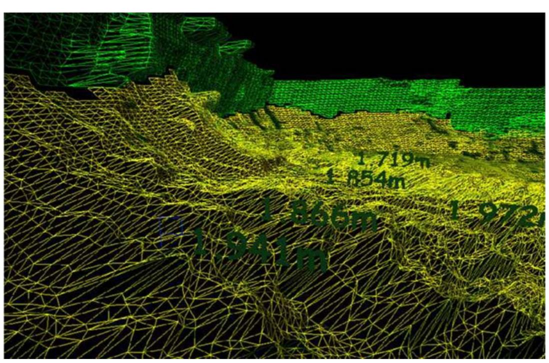

Fig. 30. Illustration of reconstruction with triangle; the data indicate the depth of the points at the flags

Acknowledgments

The writers thank the anonymous reviewers for their comments and advice. The research was supported by a grant from the major program of the Science and Technology Commission of Shanghai Municipality (Grant No. 04DZ12006), by NSFC (Grant No. 50705054), and by the Science Foundation for the Youth Teachers of Shanghai Jiaotong University (China).

References

Alshawbkeh, Y., and Stuttgart, N. (2005). "Using terrestrial laser scanning for the 3D reconstruction of Petra/Jordan." *Proc., Photogrammetric Week*, 39–47.

Amenta, N., Bern, M., and Kamvysselis, M. (1998). "A new Voronoi-based surface reconstruction algorithm," *Proc., SIGGRAPH '98*, ACM, New York, 415–421.

Arayici, Y. (2007). "An approach for real world data modelling with the 3D terrestrial laser scanner for built environment." *Autom. Constr.*, 16(6), 816–829.

Besl, P., and McKay, N. (1992). "A method for registration of 3-D shapes." *IEEE Trans. Pattern Anal. Mach. Intell.*, 14(2), 239–256.

Borghese, N., Ferrigno, G., Baroni, G., Pedotti, A., Ferrari, S., and Savare, R. (1998). "Autoscan: A flexible and portable 3D scanner." *IEEE Comput. Graphics Appl.*, 18(3), 38–41.

Cha, J., Cofer, R., and Kozaitis, S. (2006). "Extended Hough transform for linear feature detection." *Pattern Recogn.*, 39(6), 1034–1043.

Ding, Y., Ping, X., Hu, M., and Wang, D. (2005). "Range image segmentation based on randomized Hough transform." *Pattern Recogn. Lett.*, 26(13), 2033–2041.

Filin, S., and Pfeifer, N. (2006). "Segmentation of airborne laser scanning data using a slope adaptive neighborhood." *ISPRS J. Photogramm. Remote Sens.*, 60(2), 71–80.

Frohlich, C., and M, M. (2006). "Terrrestrial laser scanning-new perspectives in 3D surveying." *Int. Arch. Photogramm. Remote Sens. Spat. Inf. Sci.*, 36, 7–13.

González, E., Díaz-Pache, F., Mosquera, L., and Agudo, J. (2007). "Bi-dimensional measurement of an underwater sediment surface using a 3D-scanner." *Opt. Laser Technol.*, 39(3), 481–489.

Gregor, J., and Whitaker, R. (2001). "Indoor scene reconstruction from sets of noisy range images." *Graphical Models*, 63(5), 304–332.

Huber, D., and Hebert, M. (2003). "Fully automatic registration of multiple 3D data sets." *Image Vis. Comput.*, 21(7), 637–650.

Jiang, X., and Bunke, H. (1999). "Edge detection in range images based on scan line approximation." *Comput. Vis. Image Underst.*, 73(2), 183–199.

Kobbelt, L., and Botsch, M. (2004). “A survey of point-based techniques in computer graphics.” *Comput. Graph.*, 28(6), 801–814.
Kodaki, K., Nakano, M., and Maeda, S. (1997). “Development of the automatic system for pneumatic caisson.” *Autom. Constr.*, 6(3), 241–255.
Levoy, M., et al. (2000). “The Digital Michelangelo Project: 3D scanning of large statues,” *Int. Conf. on Computer Graphics and Interactive Tech.*, ACM/Addison-Wesley, New York, 131–144.
Li Q. Y., Wang N. C., and Y, Y. D. (2001). *Numerical analysis*, Huazhong Univ. of Science and Technology, Hubei Province, Wuhan.
Liu, Y., and Rodrigues, M. (2002). “Geometrical analysis of two sets of 3D correspondence data patterns for the registration of free-form shapes.” *J. Intell. Robotic Syst.*, 33(4), 409–436.
Meyer, A., and Marin, P. (2004). “Segmentation of 3D triangulated data points using edges constructed with a C1 discontinuous surface fitting.” *Comput.-Aided Des.*, 36(13), 1327–1336.
Peng, F. L., Sun, D. X., and M, O. (2003). “Information construction of unmanned pneumatic caisson.” *Geotech. Eng.*, 15(3), 29–32.
Rusinkiewicz, S., Hall-Holt, O., and Levoy, M. (2002). “Real-time 3D model acquisition.” *ACM Trans. Graphics*, 21(3), 438–446.
Salvi, J., Matabosch, C., Fofi, D., and Forest, J. (2007). “A review of recent range image registration methods with accuracy evaluation.” *Image Vis. Comput.*, 25(5), 578–596.
Schall, O., and Samozino, M. (2005). “Surface from scattered points: A brief survey of recent developments,” *Proc., 1st Int. Workshop Towards Semantic Virtual Environments*, MIRALab, Villars, Switzerland, 138–147.
Shih, N., Wang, H., Lin, C., and Liau, C. (2007). “3D scan for the digital preservation of a historical temple in Taiwan.” *Adv. Eng. Software*, 38(7), 501–512.
Sithole, G., and Vosselman, G. (2006). “Bridge detection in airborne laser scanner data.” *ISPRS J. Photogramm. Remote Sens.*, 61(1), 33–46.
Stamos, I., and Leordeanu, M. (2003). “Automated feature-based range registration of urban scenes of large scale.” *IEEE Computer Society Conf. on Computer Vision and Pattern Recognition*, Citeseer, 555C561.
Tognola, G., Parazzini, M., Svelto, C., Ravazzani, P., and Grandori, F. (2003). “A fast and reliable system for 3D surface acquisition and reconstruction.” *Image Vis. Comput.*, 21(3), 295–305.
Tubic, D., Hebert, P., and Laurendeau, D. (2003). “3D surface modeling from range curves,” *IEEE Computer Society Conf. on Computer Vision and Pattern Recognition*, IEEE, Piscataway, N.J.
Williams, J., Bennamoun, M., and Latham, S. (1999). “Multiple view 3D registration: A review and a new technique.” *Proc.*, *IEEE Trans. Syst. Man Cybern.*, 3, 497–502.
Yu, S., Sukumar, S., Koschan, A., Page, D., and Abidi, M. (2007). “3D reconstruction of road surfaces using an integrated multi-sensory approach.” *Opt. Lasers Eng.*, 45(7), 808–818.